Identification of nuclear effects in neutrino-carbon interactions at low momentum transfer

P.A. Rodrigues,[1] J. Demgen,[2] E. Miltenberger,[2] J. Leistico,[2]
A. Lovlein,[2] R. Gran,[2] and More signatories here[3]

(MINERvA Collaboration)

[1]*University of Rochester, Rochester, New York 14627 USA*
[2]*Department of Physics, University of Minnesota – Duluth, Duluth, Minnesota 55812, USA*
[3]*Your University, your state or nation here*

(Dated: October 30, 2015)

Abstract

Neutrino-carbon scattering data at low three-momentum transfer from the MINERvA neutrino experiment are analyzed to isolate a sample of charged-current ν_μ interactions. For the first time in a neutrino experiment, the observed hadronic energy is combined with muon kinematics to permit the separation of the quasielastic and Δ resonance processes and allow clear identification of multi-nucleon effects. A major suppression of the cross section at very low energy transfer matches the screening effect of long-range nucleon correlations, while an addition to the event rate in the dip region between the peaks of the quasielastic and Δ resonance processes is needed to describe the data. These additional events are found to have an enhanced population of multi-proton final states. Predictions of a two-particle, two-hole contribution to the cross section have both properties. The measured double-differential cross section $\mathrm{d}^2\sigma/\mathrm{d}E_{\mathrm{avail}}\mathrm{d}q_3$ enables further investigation of details of the cross section and nuclear models.

PACS numbers: 13.15.+g,25.30.Pt

The environment of the nucleus modifies neutrino scattering cross sections, compared to free nucleons and deuterium. Fermi-gas models [1] are still widely used, but consider only simple elements such as Fermi motion and Pauli-blocking. Such models are unable to consistently describe high statistics data for neutrino scattering from oxygen [2], carbon [3–8], and iron [9], especially for processes at the lowest three-momentum transfer such as quasielastic (QE) and Δ resonance production. The prevailing interpretation for these discrepancies is that more detailed nuclear models are required.

Missing nuclear effects in the QE and Δ region, or missing an entire process such as two-particle, two-hole (2p2h) contributions, is a barrier [10–15] to the precision measurement of neutrino oscillation parameters by current and future accelerator-based experiments [16–20]. The effect is especially acute when the lepton kinematics or final state content affect neutrino energy reconstruction or might affect neutrinos and anti-neutrinos differently. Uncertainties in the nuclear modeling also prevent investigation into other fundamental quantities like the nucleon axial form factor.

This letter presents the first analysis of neutrino scattering data to isolate the kinematics of the dip region between the peaks of the QE and Δ resonance processes, and confirms specific beyond-Fermi gas model effects and their energy dependence. This analysis, of data from the MINERvA experiment, clearly identifies a suppression of the cross section at low energy transfer due to long range nucleon-nucleon correlations, such as those computed [21, 22] using the Random Phase Approximation (RPA) technique. The data also give strong evidence of a process with multiple protons in the final state, such as from a predicted 2p2h process [22, 23] with energy transfer in the dip region.We present the data as a double differential cross section for further comparisons to interaction models.

A typical approach in previous investigations of nuclear effects in neutrino scattering has been to select a sample of QE events and measure the final-state charged lepton kinematics, and use them to infer Q^2, the square of the four-momentum transferred to the nucleus. Predicted RPA and 2p2h effects overlap [24] in Q^2, despite distinctly different kinematics. Without a mono-energetic neutrino beam or detailed convolution with the flux, model elements are difficult to distinguish with muon kinematics only.

Reconstructing hadronic energy, in addition to muon kinematics, permits an electron scattering (e, e')-style analysis of the neutrino energy E_ν plus a pair of variables which separate QE and Δ events: either Q^2 and hadronic invariant mass W, or energy transfer q_0

and the magnitude of three-momentum transfer $q_3 = |\vec{q}|$ to the nucleus. The latter basis is used in this letter, to avoid the model dependence inherent in producing an unfolded W cross section. To avoid model dependence in unfolding to true q_0, we define a similar quantity, the available hadronic energy E_{avail}: the energy from all charged and electromagnetic particles in the hadronic system except neutrons. This minimizes the correction from the model for the nucleon removal energy and unobserved neutrons, and allows the report of a double-differential cross section $\mathrm{d}^2\sigma/\mathrm{d}E_{\mathrm{avail}}\mathrm{d}q_3$. In detail, E_{avail} is defined as the sum of proton kinetic energy, charged pion kinetic energy, neutral pion total energy, electron and photon energy. Because neutrons are excluded, the precision of this estimator has small dependence on the particle content of the system (and therefore the interaction model) and depends mostly on the well-simulated properties of such particles as they leave the interaction point and travel through the detector.

These data are taken from the 2009 to 2012 MINERvA exposure to the NuMI beam [25] with 3.33×10^{20} protons on target. In the NuMI beam, 120 GeV protons interact with a graphite target, producing charged mesons which are focused toward the MINERvA detector by a pair of magnetic horns. These mesons decay to neutrinos in a decay pipe filled with helium, leading to a neutrino spectrum which peaks at 3.5 GeV. Compared to prior MINERvA publications, updates to the simulation of the neutrino beam and tuning to available thin-target hadron production data [26–29] to produce the predicted neutrino flux.

An inclusive sample of ν_μ charged-current interactions is selected using events that originate in MINERvA's 5.57 ton active-tracker fiducial volume [30], which consists of planes of triangular scintillator strips with a 3.4 cm base and 1.7 cm height which are up to 2 m long. Hydrogen, carbon, and oxygen account for 7.5%, 88%, and 3.2% of the target nucleons. The planes are hexagonal and alternate between three orientations (0° and ±60°) around the beam direction. This enables an excellent reconstruction of the interaction point and muon track angle in three dimensions, even when other activity overlaps the muon in one view. The MINOS near detector [31], a magnetized iron spectrometer located downstream of MINERvA, provides muon momentum measurement and sign selection.

Event kinematics are reconstructed using the measured energy and angle of the muon and the measured energy deposited by hadrons in the detector. The selection requires that muons originate in the fiducial region and are matched to reconstructed muons in the MINOS

Near Detector. Their energy is measured from their range if the muon stops in MINOS, or by curvature in the MINOS magnetic field otherwise. That energy in MINOS is added to an estimate from the muon's range in MINERvA to form E_μ and p_μ, the muon energy and momentum. The muon angle θ_μ is measured by tracking the muon in MINERvA from the interaction point. To produce a cross section based only on data in regions with good muon acceptance, we require $\theta_\mu < 20$ degrees and $E_\mu < 1.5$ GeV, though the restriction has negligible effect on this analysis.

The hadronic energy is reconstructed from the summed energy in the detector not associated with the muon track. The Monte Carlo simulation (MC) is used to obtain a correction as a function of this summed energy to the true energy transfer q_0. The correction depends significantly on the neutrino interaction model, especially the predicted neutron content of the final state. The rest of the kinematics are neutrino energy $E_\nu = E_\mu + q_0$, square of the four-momentum transfer $Q^2 = 2E_\nu(E_\mu - p_\mu \cos\theta_\mu) - \text{Mass}_\mu^2$, and the three-momentum transfer $q_3 = \sqrt{Q^2 + q_0^2}$. Model dependence from neutron content is a smaller part of q_3 because the muon energy and angle are significant. The resolution of q_3 is still dominated by the resolution of q_0. The detector's simulated response to protons and pions with the sub-GeV energies of the low-q_3 sample agrees with data from a hadron test beam experiment [32]. Constraints on calorimetry and Birks' suppression for MINERvA scintillator are used to tune the simulation and set the uncertainty scale on the single-particle response.

The event selection is completed by requiring $2 < E_\nu < 6$ GeV, an interval chosen to span the peak of the neutrino flux. The average energy of the sample is 3.9 GeV. The sample is further subdivided into six regions of q_3 from 0 to 0.8 GeV. Another sample from $6 < E_\nu < 20$ GeV allows investigation of the energy dependence of the cross section.

We estimate E_{avail} using just the calorimetric sum of energy not associated with the muon measured in the central tracker region and the electromagnetic calorimeter (ECAL) region immediately downstream of the tracker. Other tracking and calorimetric regions of the MINERvA detector contain activity from neutrons and photons, but also from unrelated beam activity, a mix that degrades the resolution at such low momentum transfers.

The distribution of reconstructed E_{avail} is shown in Fig. 1 and compared to the MC simulation. The shapes for two regions of q_3 show the same discrepancies: an overprediction of QE events and underprediction of events in the dip between the QE and Δ processes. The neutrino interaction model is from GENIE 2.8.4 [33]. Our inclusive charged current

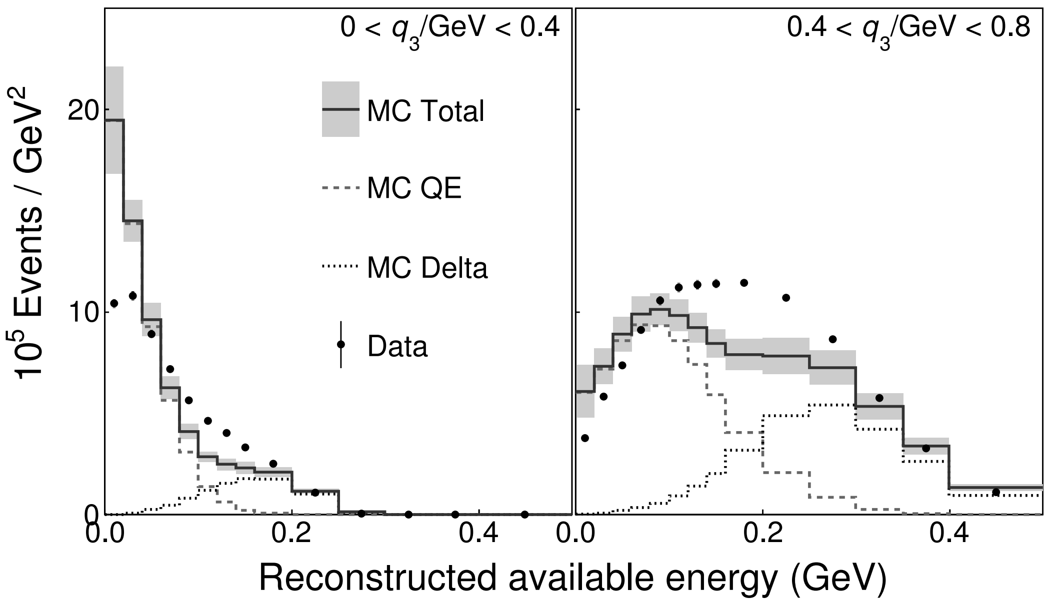

FIG. 1: Reconstructed E_{avail} compared to the default MC (with reduced pion production) for two ranges of reconstructed q_3: $q_3 < 0.4$ GeV (left) and for $0.4 < q_3 < 0.8$ GeV (right). The MC prediction for the QE process is shown by the dashed line, and for Δ resonance production by the dotted line, illustrating the location of the dip region. Data are shown with statistical uncertainty only, which is almost invisible. The absolutely normalized MC is shown with systematic uncertainties.

selection includes events with a pion in the final state, which have been shown in previous MINERvA analyses to be overpredicted by GENIE [8, 34]. We use these MINERvA results to further modify the MC prediction: The one-pion neutrino-neutron non-resonant component is reduced by 75%, and the total rate of pion production with $W < 1.8$ GeV is further reduced by 10%. Coherent pion production with $E_\pi < 450$ MeV is also reduced by 50%. This combination is the default model in this letter.

To study additional effects of the nucleus, we modify the quasielastic process with the RPA effect from the calculation of Nieves *et al.* [21]. A two-dimensional correction in (q_0, q_3) is formed from the ratio of cross sections between the model with RPA effects and the model without RPA. That correction factor is then applied to the GENIE quasielastic cross section. This technique does not include the small effect from using a local Fermi gas. It does include a short range correlation effect, but we do not simulate the presence of the spectator nucleon

[35] in the final state.

We also add a 2p2h process on carbon and oxygen to the simulation, using the model of Nieves *et al.* [23, 24]. The cross section depends on q_0, q_3, and whether the initial nucleon pair is proton-neutron or neutron-neutron. This calculation includes only the QE-like (no pion in the final state) contributions, but does include interactions with Δ kinematics.

Explicit hadron kinematics are added to the 2p2h model using a strategy similar to that of [36], documented in detail in [37]. The nucleon pair is drawn from the standard GENIE Fermi gas distribution, given one unit charge and the momentum and energy transfer, less two units of 25 MeV nucleon removal energy. It is "decayed" isotropically and back to back in its center of momentum frame, then boosted back to the nucleus (lab) rest frame, which is a good approximation [38] to a full calculation. The resulting nucleons are passed to the GENIE intranuclear rescattering model where their number and energy may change.

An unfolding procedure [39] with four iterations is applied in two dimensions to translate the data from reconstructed quantities to true $(E_{\rm avail}, q_3)$. The unfolding matrix is diagonal in each bin of q_3, with the bin width chosen so 25% or more of the events are in the on-diagonal entries in the matrix, and 60% when the adjacent two entries are included. The MC is used to correct for the acceptance of the fiducial volume, the efficiency of the MINOS muon match, and the subtraction of small (3%) neutral current and μ^+ backgrounds. Dividing by the flux and number of targets results in the double-differential cross section $\mathrm{d}^2\sigma/\mathrm{d}E_{\rm avail}\mathrm{d}q_3$, shown in Fig. 2 for six regions of q_3. The cross section and the flux used is available as supplementary material.

Both the q_3 and the $E_{\rm avail}$ estimators have mild dependence on the interaction model. The results in this paper, especially the migration matrix used for the unfolding, are produced using the fully modified model rather than the default. In principle, starting with the best model produces better unfolding results and systematic uncertainties overall. Since neither model provides a complete description of the data, we also extract the cross section using the default model, and take the difference between the two as a systematic uncertainty. This is the largest contributor (10%) to the systematic uncertainty for q_3 below 0.4 GeV. The flux uncertainty (6%) is the next largest, followed by hadronic and muon energy scales. The total uncertainty ranges from 10% at high q_3 and high $E_{\rm avail}$ through the dip region, growing to 20% at the lowest $E_{\rm avail}$ and q_3.

The discrepancy seen in the unfolded data in Fig. 2 is much smaller with these model

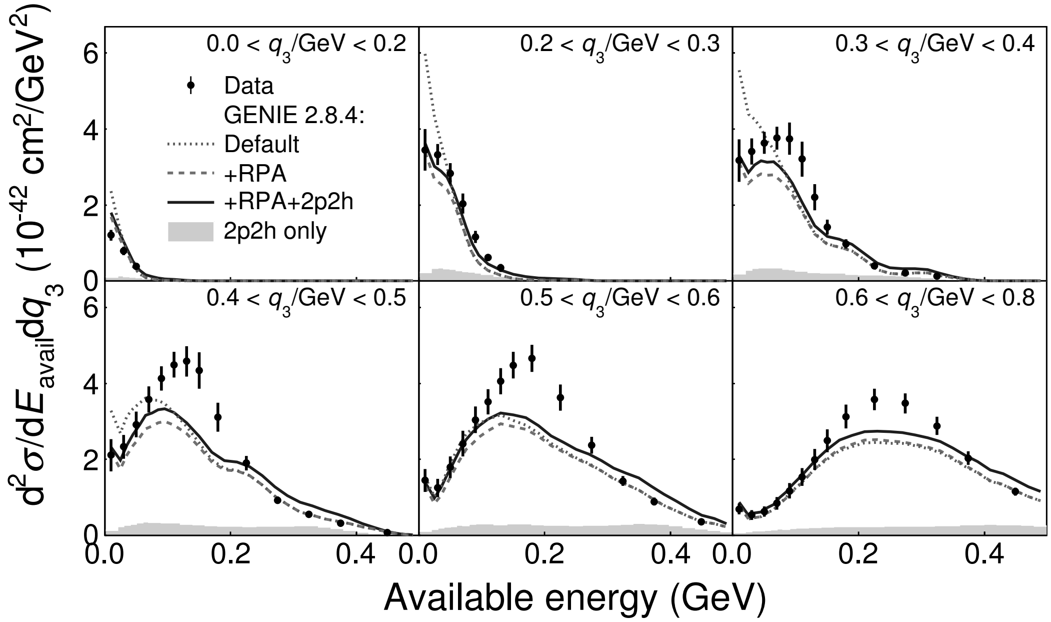

FIG. 2: Double-differential cross section $\mathrm{d}^2\sigma/\mathrm{d}E_{\mathrm{avail}}\mathrm{d}q_3$ in six regions of q_3. The cross section is compared to the GENIE 2.8.4 model with reduced pion production (small dot line), the same with RPA suppression (long-dashed), and then combined with a QE-like 2p2h component (solid). The 2p2h component is shown separately as a shaded region. GENIE predicts a delta-function at zero available energy in each bin, which is not shown.

additions. The RPA suppression has a significant effect on the lowest E_{avail} bins, and produces very good agreement. The model that includes RPA is theoretically motivated and the lowest Q^2 behavior of the QE process is almost completely tuned to data: neutron decay for the axial form factor $F_A(Q^2 = 0)$, and muon capture on nuclei [21] for the long-range correlation effect. The χ^2 from comparing the reconstucted MC and the data, with the full covariance matrix, decreases from 885 (for 61 degrees of freedom) for the default MC to 519 when the RPA effects are added. The simulated QE-like 2p2h contribution spans the horizontal axis and mitigates some of the discrepancy in the dip region between the QE and Δ, further improving the agreement in shape from the QE to the dip region. The resulting χ^2 is improved further to 489. The prediction still does not fully describe the data, especially in the dip and Δ regions.

Another sample is created with the energy range $6 < E_\nu < 20$ GeV. The unmodeled shape differences between the data and MC, for high and low energy, are consistent with no energy dependence within statistical uncertainties. The proposed model enhancements also have negligible energy dependence. Differences in the normalization are consistent with the energy dependence of the flux. An unmodeled energy dependence as large as zero 2p2h component above 5 GeV is disfavored by more than three standard deviations, with the muon energy scale being the largest contributing systematic uncertainty. This observation is also an important confirmation that the low-ν method [40–43] or the asymptotic behavior of the QE process may be an effective method to constrain the relative E_ν dependence of the neutrino flux.

The 2p2h process transfers energy and momentum to two nucleons. Those two nucleons, possibly more with final state interactions (FSI), will be ejected from the nucleus. This is in contrast to the QE, Δ, and coherent pion interactions which produce a single recoiling nucleon, nucleon and pion, and only a pion, respectively (before FSI). Nieves model predicts [24] that two proton final states outnumber proton plus neutron final states for neutrino mode data. Even with FSI reinteractions, the 2p2h process should have one more nucleon, on average, than the other processes. Such an observation was previously reported [6] by MINERvA, inferred from the energy spectrum of hadronic activity near the vertex.

It is possible to identify protons in MINERvA using the Bragg peak at the end of their range in scintillator. Even if a proton has too little energy to be tracked, it is likely to deposit 20 MeV or more in a single scintillator strip. The 20 MeV deposit will not be far from the event interaction point; for the lowest energy protons it may be the same scintillator strip where the interaction occurred. Pions and neutrons are likely to leave the interaction region ($\pm$170mm in the beam direction and within $\pm$83 mm transverse) and leave none or only lower energy deposits. When fully simulated, QE and Δ production events with a pion from the dip region of the $0.4 < q_3 < 0.8$ sample produce an average of 1.0 strips with activity more than 20 MeV in the interaction region. Two-nucleon events from the 2p2h process or Δ interactions that lose their pion to FSI produce 1.6 and 1.5 strips with 20 MeV, respectively.

The default MC does not have enough protons in the dip region, specifically the ranges in Fig. 1 from 0.08 to 0.16 (0.14 to 0.26) GeV in the low (high) q_3 distributions. Table I shows that variations of the MC provide better description of the data with each model modification. The simulation is hardly altered by the RPA suppression that dominates the lowest energy transfer events, below the dip region. The addition of the 2p2h component makes the most dramatic change. The reduction of pion production compared to the GENIE

$0 < q_3 < 0.4$ GeV	0	1	2	3+	χ^2	χ^2
MC GENIE 2.8.4	38.0	45.0	15.9	1.1	17.4	
MC-π "default"	34.0	47.6	17.2	1.2	9.5	
MC-π-RPA	34.4	47.2	17.2	1.2	10.2	
MC-π-RPA+2p2h	30.5	48.1	19.7	1.8	5.2	
Data (3670 events)	29.6	46.8	20.8	2.9		
Binomial stat error	0.8	0.8	0.7	0.3		
Systematic uncertainty	2.6	2.3	2.1	0.7	3 dof	
$0.4 < q_3 < 0.8$ GeV						
MC GENIE 2.8.4	37.2	36.1	19.0	7.8	7.6	18.5
MC-π "default"	35.7	36.7	19.5	8.1	5.8	13.7
MC-π-RPA	35.9	36.6	19.4	8.1	5.9	14.0
MC-π-RPA+2p2h	33.9	36.2	20.7	9.3	1.7	7.3
Data (17756 events)	31.5	35.6	22.1	10.8		
Binomial stat error	0.3	0.4	0.3	0.2		
Systematic uncertainty	2.1	0.9	1.2	1.4	3 dof	6 dof

TABLE I: Percent of events with zero, one, two, and three or more strips with at least 20 MeV of activity near the interaction point for the dip region of two q_3 subsamples. The rows show the results for the GENIE 2.8.4 MC and the three modifications of the MC, followed by results for the data with statistical and systematic uncertainties. The final two columns show the evolution of the χ^2 between the data and each model change; first for the subsamples separately, and the final column is for the combination of the two subsamples.

default also increases the relative number of multi-proton events. The region above the dip (dominated by resonances and unsimulated 2p2hπ interactions) show all the same trends. Below the dip (dominated by QE) the agreement is most improved with the addition of the RPA suppression; sensitivity to multiple protons is reduced due to the QE background and the protons' lower energy.

The most significant systematic uncertainty is from the value [32] for Birks' parameter used in the MC. Uncertainties from the GENIE final state interaction model, especially pion absorption, change the multi-nucleon content and are also significant, but the 1σ uncertainty produces effects that are a factor of three smaller than this model for 2p2h reactions. The shape of the pion energy spectrum reported in [8] is especially sensitive to the FSI model and is adequately described with GENIE and its FSI uncertainties. The hadron energy scale [32] can distort the MC to better describe one subsample or the other, but not both simultaneously, reducing its significance. The uncertainties shown in Table I are from the diagonal terms of the covariance matrix, but the χ^2 between the data and each model is computed using the full covariance.

The significantly improved agreement, even using a single 2p2h model with a simplified hadronic system, is additional evidence that a multi-nucleon component is present in the data. Refinements to this 2p2h model, or other models [22, 44] (not currently available for full simulation) may predict more multi-proton events, or with different kinematics, which may further improve the description of the data.

An alternate approach that uses the superscaling hypothesis [44, 45] to describe the 1p1h process in electron scattering data empirically picks up the short range correlation effects. Relative to a Fermi gas model, and the model used in this letter, this approach produces a migration of $\sim$15% of the QE cross section from the QE peak toward the dip region. Combined with a post-hoc final state that includes the spectator nucleon [46] and an explicit 2p2h process like the one simulated here, this could further improve the description of the data in the dip region. The cross sections and indications of the proton final state content presented here are uniquely equivalent to the electron scattering process that superscaling and 2p2h models were originally built to describe, and will lead to implementations broadly available with new accuracy for neutrino experiments.

In acknowledgement, we are grateful for the authors of the RPA and 2p2h models for making the code for their calculations available for study and incorporation into this analysis. This work was supported by the Fermi National Accelerator Laboratory under US Department of Energy contract No. DE-AC02-07CH11359 which included the MINERvA construction project. Construction support was also granted by the United States National Science Foundation under Grant PHY-0619727 and by the University of Rochester. Support for scientists for this specific publication was granted by the United States National Science Foundation under Grant PHY-1306944. Support for participating scientists was provided by NSF and DOE (USA) by CAPES and CNPq (Brazil), by CoNaCyT (Mexico), by CON-

ICYT (Chile), by CONCYTEC, DGI-PUCP and IDI/IGI-UNI (Peru), by Latin American Center for Physics (CLAF) and by RAS and the Russian Ministry of Education and Science (Russia). We thank the MINOS Collaboration for use of its near detector data. Finally, we thank the staff of Fermilab for support of the beamline, the detector, and the computing infrastructure.

[1] R. A. Smith and E. J. Moniz, Nucl.Phys. **B43**, 605 (1972).

[2] R. Gran *et al.* (K2K Collaboration), Phys.Rev. **D74**, 052002 (2006), arXiv:hep-ex/0603034 [hep-ex] .

[3] V. Lyubushkin *et al.* (NOMAD Collaboration), Eur.Phys.J. **C63**, 355 (2009), arXiv:0812.4543 [hep-ex] .

[4] X. Espinal and F. Sanchez (K2K Collaboration), AIP Conf. Proc. **967**, 117 (2007).

[5] A. Aguilar-Arevalo *et al.* (MiniBooNE Collaboration), Phys.Rev. **D81**, 092005 (2010), arXiv:1002.2680 [hep-ex] .

[6] G. Fiorentini, D. Schmitz, P. Rodriguez, *et al.* (MINERvA Collaboration), Phys. Rev. Lett. 111, **022502** (2013), 10.1103/PhysRevLett.111.022502, arXiv:1305.2243 [hep-ex] .

[7] T. Walton *et al.* (MINERvA), Phys. Rev. **D91**, 071301 (2015), arXiv:1409.4497 [hep-ex] .

[8] B. Eberly *et al.* (MINERvA Collaboration), (2014), arXiv:1406.6415 [hep-ex] .

[9] P. Adamson *et al.* (MINOS Collaboration), Phys.Rev. **D91**, 012005 (2015), arXiv:1410.8613 [hep-ex] .

[10] J. Nieves, F. Sanchez, I. Ruiz Simo, and M. Vicente Vacas, Phys. Rev. **D85**, 113008 (2012), arXiv:1204.5404 [hep-ph] .

[11] O. Lalakulich, U. Mosel, and K. Gallmeister, Phys.Rev. **C86**, 054606 (2012), arXiv:1208.3678 [nucl-th] .

[12] M. Martini, M. Ericson, and G. Chanfray, Phys.Rev. **D87**, 013009 (2013), arXiv:1211.1523 [hep-ph] .

[13] U. Mosel, O. Lalakulich, and K. Gallmeister, Phys.Rev.Lett. **112**, 151802 (2014), arXiv:1311.7288 [nucl-th] .

[14] P. Coloma, P. Huber, C.-M. Jen, and C. Mariani, Phys. Rev. **D89**, 073015 (2014), arXiv:1311.4506 [hep-ph] .

[15] M. Ericson and M. Martini, Phys. Rev. **C91**, 035501 (2015), arXiv:1501.02442 [nucl-th] .

[16] P. Adamson *et al.* (MINOS Collaboration), Phys.Rev.Lett. (2013), 10.1103/PhysRevLett.110.171801, arXiv:1301.4581 [hep-ex] .

[17] K. Abe *et al.* (T2K), Phys. Rev. **D91**, 072010 (2015), arXiv:1502.01550 [hep-ex] .

[18] D. S. Ayres *et al.* (NOvA Collaboration), (2004), arXiv:hep-ex/0503053 [hep-ex] .

[19] R. Acciarri *et al.*, *A Proposal for a Three Detector Short-Baseline Neutrino Oscillation Program for the Fermilab Booster Neutrino Beam*, Tech. Rep. (2015) arXiv:1503.01520 [hep-ex] .

[20] C. Adams *et al.* (LBNE) (2013) arXiv:1307.7335 [hep-ex] .

[21] J. Nieves, J. E. Amaro, and M. Valverde, Phys. Rev. **C70**, 055503 (2004), arXiv:nucl-th/0408005 [nucl-th] .

[22] M. Martini, M. Ericson, G. Chanfray, and J. Marteau, Phys. Rev. **C80**, 065501 (2009), arXiv:0910.2622 [nucl-th] .

[23] J. Nieves, I. Ruiz Simo, and M. Vicente Vacas, Phys. Rev. **C83**, 045501 (2011), arXiv:1102.2777 [hep-ph] .

[24] R. Gran, J. Nieves, F. Sanchez, and M. Vicente Vacas, Phys.Rev. **D88**, 113007 (2013), arXiv:1307.8105 [hep-ph] .

[25] P. Adamson *et al.*, Nucl.Instrum.Meth.A (2015), arXiv:1507.06690 [physics.acc-ph] .

[26] C. Alt *et al.* (NA49), Eur. Phys. J. **C49**, 897 (2007), arXiv:hep-ex/0606028 [hep-ex] .

[27] S. P. Denisov, S. V. Donskov, Yu. P. Gorin, R. N. Krasnokutsky, A. I. Petrukhin, Yu. D. Prokoshkin, and D. A. Stoyanova, Nucl. Phys. **B61**, 62 (1973).

[28] A. S. Carroll *et al.*, Phys. Lett. **B80**, 319 (1979).

[29] J. V. Allaby *et al.* (IHEP-CERN), Phys. Lett. **B30**, 500 (1969).

[30] L. Aliaga *et al.* (MINERvA Collaboration), Nucl.Instrum.Meth. **A743**, 130 (2014), arXiv:1305.5199 [physics.ins-det] .

[31] D. G. Michael *et al.* (MINOS Collaboration), Nucl.Instrum.Meth. **A596**, 190 (2008), arXiv:0805.3170 [physics.ins-det] .

[32] L. Aliaga *et al.* (MINERvA), Nucl. Instrum. Meth. **A789**, 28 (2015), arXiv:1501.06431 [physics.ins-det] .

[33] C. Andreopoulos, A. Bell, D. Bhattacharya, F. Cavanna, J. Dobson, S. Dytman, H. Gallagher, P. Guzowski, R. Hatcher, P. Kehayias, A. Meregaglia, D. Naples, G. Pearce, A. Rubbia,

M. Whalley, and T. Yang, Nuclear Instruments and Methods in Physics Research Section A: Accelerators, Spectrometers, Detectors and Associated Equipment **614**, 87 (2010), Program version 2.8.4 used here.

[34] A. Higuera *et al.* (MINERvA), Phys. Rev. Lett. **113**, 261802 (2014), arXiv:1409.3835 [hep-ex] .

[35] K. S. Egiyan *et al.* (CLAS), Phys. Rev. Lett. **96**, 082501 (2006), arXiv:nucl-ex/0508026 [nucl-ex] .

[36] J. T. Sobczyk, Phys.Rev. **C86**, 015504 (2012), arXiv:1201.3673 [hep-ph] .

[37] R. Gran and J. Schwehr, *TN061 Implementation of Nieves MEC model in GENIE*, Tech. Rep. (MINERvA docdb:11276, 2015).

[38] I. R. Simo, C. Albertus, J. E. Amaro, M. B. Barbaro, J. A. Caballero, and T. W. Donnelly, Phys. Rev. **D90**, 053010 (2014), arXiv:1407.7122 [nucl-th] .

[39] G. D'Agostini, Nucl.Instrum.Meth. **A362**, 487 (1995).

[40] S. R. Mishra, in *Proceedings of the Workshop on Hadron Structure Functions and Parton Distributions*, edited by D. Geesaman *et al.* (World Scientific, 1990) pp. 84–123.

[41] W. Seligman, *Ph.D. Thesis*, Ph.D. thesis, Columbia University (1997), Nevis 292.

[42] P. Adamson *et al.* (MINOS), Phys. Rev. **D81**, 072002 (2010), arXiv:0910.2201 [hep-ex] .

[43] A. Bodek, U. Sarica, D. Naples, and L. Ren, Eur. Phys. J. **C72**, 1973 (2012), arXiv:1201.3025 [hep-ex] .

[44] G. D. Megias *et al.*, Phys. Rev. **D91**, 073004 (2015), arXiv:1412.1822 [nucl-th] .

[45] J. E. Amaro, M. B. Barbaro, J. A. Caballero, T. W. Donnelly, A. Molinari, and I. Sick, Phys. Rev. **C71**, 015501 (2005), arXiv:nucl-th/0409078 [nucl-th] .

[46] A. Bodek, M. E. Christy, and B. Coopersmith, Eur. Phys. J. **C74**, 3091 (2014), arXiv:1405.0583 [hep-ph] .